Author Manuscript

Author Manuscript

Author Manuscript

Author Manuscript

HHS Public Access

Author manuscript

Cancer Lett. Author manuscript; available in PMC 2023 December 01.

Published in final edited form as:

Cancer Lett. 2022 December 01; 550: 215924. doi:10.1016/j.canlet.2022.215924.

Structural or functional defects of PTEN in urothelial cells lacking P53 drive basal/squamous-subtype muscle-invasive bladder cancer

Feng He[a,d,1], **Fenglin Zhang**[a,1], **Yi Liao**[a,1], **Moon-shong Tang**[b], **Xue-Ru Wu**[a,c,d,*]

[a]Department of Urology, New York University School of Medicine, New York, NY 10016, USA

[b]Department of Environmental Medicine, New York University School of Medicine, New York, NY 10016, USA

[c]Department of Pathology, New York University School of Medicine, New York, NY 10016, USA

[d]Veterans Affairs New York Harbor Healthcare System, Manhattan Campus, New York, NY 10010, USA

Abstract

Muscle-invasive bladder cancer (MIBC) exhibits strong inter- and intra-tumor heterogeneity that affects biological behaviors, therapeutic responses, and prognoses. Mutations that activate RTK-RAS-PI3K and inactivate P19-P53-P21 coexist in 60-70% of MIBC. By time-controlled ablation of *Tp53* and *Pten*, singly or combined, in adult mouse urothelium, we found that *Tp53* loss alone produced no abnormality. While *Pten* loss elicited hyperplasia, it synergized with *Tp53* loss to trigger 100% penetrant MIBC that exhibited basal/squamous features that resembled its human counterpart. Furthermore, PTEN was inactivated in human MIBC cell lines and specimens primarily by hyperphosphorylation of the C-terminus. Mutated or tailless PTEN incapable of C-terminal phosphorylation demonstrated increased inhibition of proliferation and invasion than full-length PTEN in cultured MIBC cells. In xenograft and transgenic mice, tailless PTEN, but not full-length PTEN, prevented further growth in established tumors. Collectively, deficiencies of both PTEN and P53 drive basal/squamous subtype MIBC. PTEN is inactivated by C-terminal hyperphosphorylation, and this modification may serve as a biomarker for subtyping MIBC and predicting tumor progression. Tailless PTEN is a potential molecular therapeutic for tumors, such as bladder cancer (BC), that can be readily accessed.

Keywords

urothelial carcinoma; molecular subtypes; genetic drivers; *Pten*; *Tp53*; PTEN phosphorylation

[*]Send editorial correspondence to: Dr. Xue-Ru Wu, Department of Urology, New York University School of Medicine, Veterans Affairs Medical Center in Manhattan, 423 E23 Street, 6th Floor, Room 6028 West, New York, New York 10010, Tel: 212-263-4167, Fax: 212-951-5424, xue-ru.wu@med.nyu.edu.

[1]These authors contributed equally to this work.

Conflict of interest

The authors declare no conflict of interest.

Author Manuscript Author Manuscript Author Manuscript Author Manuscript

1. Introduction

Muscle-invasive bladder cancer (MIBC) is a highly aggressive form of cancer that is prone to spread to local and distant organs [1-5]. The mainstay of treatment for localized MIBC involves radical cystectomy and bilateral pelvic lymph node dissection along with, in some healthcare settings, preoperative and/or postoperative multiagent adjuvant chemotherapy [6, 7]. However, despite the loss of the bladder and the debilitating chemotherapy, both of which substantially compromise the quality of life of patients, local and distant metastases occur in up to 50% of the cases [1, 8, 9]. According to the American Cancer Society, the current 5-year survival rate of patients with regional and distant metastasis remains at 38 and 6%, respectively [8].

A major breakthrough over the past few years that holds significant promise to reduce the mortality, prolong the lifespan and improve the quality of life of patients with MIBC is the recognition that MIBC is comprised of several molecular subtypes that appear to respond differently to existing therapeutic modalities and result in different clinical outcomes [10-12]. Transcriptome profiling of human MIBC revealed that about 60% of MIBCs belong to the “luminal” subtype, which is characterized by the high expression of markers normally expressed by the differentiated luminal urothelial cells, such as cytokeratin 20 (KRT20), uroplakins, GATA Binding Protein 3 (GATA3), and Forkhead Box A1 (FOXA1). This subtype may be further divided based on the tumor histology and status of immune infiltration into “luminal papillary” (35%), “luminal infiltrated” (19%), and “luminal” (6%) subcategories [10]. Another major molecular subtype, accounting for about 35% of MIBCs, belong to the “basal/squamous” subtype that carries features typical of basal urothelial cells with high expression of cytokeratins 5 (KRT5) and 14 (KRT14) as well as squamous differentiation markers, such as cytokeratin 6 (KRT6) and desmocollin 3 (DCS3). The remaining MIBCs (approximately 6%) expresses markers that are highly abundant in neural tissues, such as SRY-Box Transcription Factor 2 (SOX2) and Distal-Less Homeobox 6 (DLX6), hence the term “neuronal” [10, 13]. Notably, the luminal MIBC has a low or predicted-low response rate to cisplatin-based neoadjuvant therapy and immune-checkpoint blockade therapy, with the exception of the luminal-infiltrated subcategory which moderately expresses programmed cell death-ligand 1 (PD-L1) and cytotoxic T-lymphocyte associated Protein 4 (CTLA-4). In contrast, a majority (60%) of basal/squamous MIBC responds well to cisplatin-based neoadjuvant therapy and, since most of these MIBC express high levels of PD-L1 and CTLA-4, they respond favorably to the immune-checkpoint blockade therapy [10]. The neuronal MIBC, which is often associated with a poor clinical outcome, may respond to etoposide and cisplatin-based neoadjuvant therapy [10, 13].

Despite the encouraging prospect that the molecular subtyping will bring precision management into MIBC, outstanding questions remain. It is unknown whether the molecular subtypes of MIBC, which are primarily based on the mRNA expression signatures, share the same genetic driver(s) or are driven by distinct genetic driver(s). Whole-genome/-exome sequencing of human MIBC revealed that activating the RTK-RAS-PI3K pathway and inactivating the P19-P53-P21 pathway are present in 89 and 71% of the cases, respectively [10, 14], making them the most frequently affected pathways in MIBC and the logical starting point for experimental validation of the genetic drivers. Emerging evidence from

Author Manuscript Author Manuscript Author Manuscript Author Manuscript

genetically engineered mice shows that, although genetic alterations in either of the two pathways elicit little to no urothelial abnormality, combined genetic alterations involving both pathways are highly tumorigenic in MIBC. Puzio-Kuter et al. showed that bi-allelic deletions of both *Pten* (which activates PI3K) and *Tp53* by intravesicle delivery of adenovirus-driven *Cre* recombinase into the bladders of loxP-flanked *Pten* and *Tp53* mice led to early-onset, fully penetrant MIBC [15]. However, molecular subtyping information was unavailable at the time. Additionally, while *Tp53* mutations and deletions occur in approximately 50% of human MIBC, mutation and deletion of *Pten* are rare, affecting only 0-6% of cases [16-19]. This indicates the possibility that alterations of players other than PTEN in the RTK-RAS-PI3K pathway collaborate with P53 alterations to drive MIBC. Alternatively, instead of mutation and deletion, PTEN could be functionally inactivated by other mechanisms in the absence of structural aberrations. Consistent with this notion, Chaux et al. found in a cohort of 156 locally MIBC that, instead of decreased expression, PTEN was in fact overexpressed, and this overexpression was significantly associated with increased tumor recurrence, progression and systemic metastases [20]. These results lent further support to our hypothesis that the functional inactivation of overexpressed PTEN occurs in a substantial portion of human MIBC and may collaborate with P53 deficiencies to induce MIBC and its subtypes.

In the present study, we assessed the *in vivo* effects of PTEN and P53 deficiencies on the genesis of MIBC and its subtypes by employing inducible knockout of *Pten* and *Tp53*, singly or in a combination, in adult mouse urothelial cells. We also assessed the C-terminal hyper-phosphorylation of PTEN – a major mechanism of functional inactivation of PTEN [21-23], with respect to its frequency and mechanisms of action in BC cell survival, apoptosis, cell-cycle progression, cell migration and invasion. Finally, we examined whether we could harness the tumor-suppressive property of experimentally engineered PTEN that is resistant to C-terminal hyper-phosphorylation as a potential therapeutic to broaden the repertoire of BC treatment.

2. Materials and Methods

2.1. Genetically engineered mice

mUpk2-rtTA-M2, previously developed in the corresponding author's laboratory, is a transgenic mouse line in which a 3.6-kB mouse *Upk2* promoter controls the urothelium-specific expression of a reverse tetracycline transactivator (modified version 2 with improved sensitivity and reduced basal activity) [24, 25]). *Tre-Cre* (Jackson Laboratory, Bar Harbor, ME, USA; [26]) is a transgenic mouse line in which the tetracycline response elements drive the expression of *Cre* recombinase. These two lines were crossed to generate a double-transgene, homozygous status and were maintained in Friend Virus B/N (FVB/N) inbred genetic background. The *mUpk2-rtTA-M2 / Tre-Cre* mice were crossed separately with (i) a floxed *Tp53* mouse line ($Tp53^{fl/fl}$) in which exons 5 and 6 of *Tp53* gene were flanked by two loxP sites (Jackson Laboratory, Bar Harbor, ME, USA) [27] or (ii) a floxed *Pten* mouse line ($Pten^{fl/fl}$) in which exon 5 of *Pten* gene was flanked by two loxP sites (Jackson Laboratory, Bar Harbor, ME, USA) [28]. From these crosses and additional intercrosses among the offspring, we obtained

Author Manuscript Author Manuscript Author Manuscript Author Manuscript

two compound mouse lines that harbored either *mUpk2-rtTA-M2* / *Tre-Cre* / *Tp53*$^{fl/fl}$ or *mUpk2-rtTA-M2* / *Tre-Cre* / *Pten*$^{fl/fl}$. To generate double *Pten* and *Tp53* inducible knockout mice, we intercrossed the aforementioned two compound mouse lines, yielding *mUpk2-rtTA-M2* / *Tre-Cre* / *Tp53*$^{fl/fl}$ / *Pten*$^{fl/fl}$ mice. All the mice were genotyped by PCR using genomic DNA isolated from tail biopsies. The oligonucleotide primers used for genotyping were: *rtTA-M2*: forward: 5′-AAGTCATTCCGCTGTGCTCT-3′; reverse: 5′-CAAAATCGTCAAGAGCGTCA-3′; *Tre-Cre:* forward: 5'-CGTACTGACGGTGGGAGAAT-3'; reverse: 5'-TGCATGATCTCCGGTATTGA-3'; for *Pten*^{fl}: Forward: 5'-CAAGCACTCTGCGAACTGAG-3'; reverse: 5'-AAGTTTTTGAAGGCAAGATGC-3'; and *Tp53*^{fl}: forward: 5′-GCTGCAGGTCACCTGTAG-3′; reverse: 5′-CATGCAGGAGCTATTACACA-3′. To perform inducible *Pten* and/or *Tp53* knockout in mouse urothelial cells, we fed adult mice (2-3 months old; both genders) a doxycycline-containing diet (20 g/kg doxycycline) *ad libitum* continuously until they were euthanized. Control mice received a regular diet without doxycycline. All the animal-related work was conducted after the approval of the protocol (#IA16-02075) by the Institutional Animal Care and Use Committee of New York University School of Medicine. All procedures were conducted in accordance with regulatory guidelines.

2.2. Human BC specimens

For western blot detection of PTEN and phosphorylated PTEN, 14 samples of non-invasive human BC from transurethral resection (seven low-grade; seven 7 high-grade) were stored in liquid nitrogen. The tissues were completely de-identified, coded (from T1-T14), and frozen until western blot analysis (see below).

2.3. Cell lines and culture

A panel of established cell lines originally derived from and representing different grades and stages of human BC were chosen for this study: RT4 (grade-1, non-invasive), RT112 (grade-2, invasive), 5637 (grade-2, invasive), 1376 (grade-3, invasive), T24 (grade-3, invasive), J82 (grade-3, invasive), UMUC3 (high-grade, invasive), TCCsup (grade-4, anaplastic, metastatic), and SCaBER (invasive, squamous cell carcinoma). All cell lines were purchased from American Type Culture Collection (ATCC; Manassas, VA, USA), except for RT112 which was obtained from MilliporeSigma (Burlington, MA, USA). The cell lines were free of mycoplasma, proven authentic by the suppliers through the identification of characteristic short-tandem repeats and were used within six months of purchase. The cell lines were cultured in the following media supplemented with 10% fetal bovine serum (FBS): RT4 and T24 in McCoy's 5a medium; RT112 and 5637 in RPMI-1640 Medium; and 1376, TCCsup, J82, UMUC3 and SCaBER in Eagle's Minimum Essential Medium. When tests were performed on the growth factor-mediated effects on PTEN phosphorylation, FBS-free or low-FBS (2%) media were used in comparison with high-FBS (10%) media. All the cell culture reagents were obtained from GIBCO - Thermo Fisher Scientific (Grand Island, NY, USA).

Author Manuscript Author Manuscript Author Manuscript Author Manuscript

2.4. Site-directed mutagenesis and domain deletion of PTEN

Two complementary sets of site-directed mutagenesis of *Pten* were conducted using QuikChange® II Site-Directed Mutagenesis Kit (Agilent Technologies, Santa Clara, CA, USA), one that converted one or more of the six C-terminal potential phosphorylation sites (T366/S370/S380/T382/T383/S385) to phosphorylation-incompatible alanine(s), and the other to phosphorylation-mimicking aspartate(s). A plasmid bearing human *Pten* cDNA (pOTB7-*Pten*, ATCC) served as a template during site-directed mutagenesis. After confirmation by DNA sequencing, all the *Pten* mutants were sub-cloned into mammalian expression vector pcDNA3. The deletion of PTEN C-terminal domain (residue 353 to 403) was achieved by PCR using PfuUltra™ High-Fidelity DNA Polymerase (Agilent Technologies, Santa Clara, CA, USA), and also sequence-verified and subcloned into pcDNA3.

2.5. Transient and stable transfection and doxycycline-induced gene expression

Transient transfection was conducted using Lipofectamin 2000 (Thermo Fisher Scientific, Waltham, MA, USA). Stable clones were selected in the presence of G418 (800 μg/mL) continuously for 14 d. To circumvent the difficulty of maintaining stable clones expressing cytotoxic tailless PTEN, we employed a tetracycline-based Tet-on system to inducibly express full-length and tailless PTEN. Thus, UMUC3 cells were first transfected and selected in G418 to stably express a pTet-On plasmid (Clontech, Mountain View, CA, USA). The stable cells were secondarily transfected with pTRE2puro-full-length PTEN or pTRE2puro-tailless PTEN and stably selected in the presence of puromycin (2 μg/mL) for 14 d. The clones that survived were subjected to inducible expression of full-length or tailless PTEN in the presence of doxycycline (0.5 μg/mL).

2.6. Cell-viability, cell-cycle, and apoptosis assays

Viability of the cultured cells was assessed using two different methods. In the first, the cell suspension was stained with 0.4% Trypan blue and the unstained (viable cells) were enumerated using a hemocytometer and tabulated. In the second, viable cells were quantified using the MTT 3-(4,5-dimethylthiazol-2-yl)-2,5-diphenyltetrazolium bromide assay (ThermoFisher Scientific, Waltham, MA, USA). The reactions were read by spectrophotometry at 570 nm and plotted against a standard curve. Cell-cycle and apoptosis was determined by staining the cultured cells with propidium iodide and Annexin V-FITC apoptosis kit (Cell Signaling, Danvers, MA, USA), respectively, followed by fluorescence-activated cell sorting. All samples were assayed in triplicate.

2.7. Tumor cell migration and invasion

Tumor cells were seeded into 12-well plates (2×10^4 cells/well) and allowed to reach 80% confluence. Wounds were introduced by scratching using sterile pipette tips. The extent of cell migration was recorded by photographing the images under phase contrast microscopy. The average distances between the leading edges of cell migration were measured, tabulated and expressed as the gaps between the edges.

For cell-invasion, BioCoat Matrigel Invasion Chamber (BD Biosciences, Franklin Lakes, NJ, USA) was used. Stable clones were seeded in 24-well cell culture chambers (2×10^4

Author Manuscript Author Manuscript Author Manuscript Author Manuscript

cells/chamber). After incubation for 36 h, the non-invading cells were removed by scraping and, the invading cells beneath the membrane were visualized using Diff-Quik stain and counted in five microscopic fields (one-center and four-peripheral).

2.8. Co-immunoprecipitation

UMUC3 cells stably harboring the mock vector, the full-length PTEN or the tailless PTEN were transduced with a lentivirus containing the FLAG-tagged wild-type P53 (P53-FLAG) and cultured in a selection media containing 0.5 μg/mL puromycin. After 24 h, the cells were harvested, washed with phosphate-buffered saline (PBS), lysed with RIPA buffer, and centrifuged at 12, 000 x g for 10 min. The supernatants were incubated with mouse anti-PTEN antibody (Novus, Littleton, CO, USA; dilution 1:200) or mouse anti-FLAG antibody (Sigma, St. Louis, MO, USA; dilution 1:200) and then Protein A/G Plus-agarose (Santa Cruz Biotechnology, Dallas, TX, USA). The beads were collected and washed in RIPA buffer and the bound proteins eluted by boiling in 1 x sodium dodecyl-sulfate polyacrylamide gel electrophoresis (SDS-PAGE) loading buffer. Western blotting was conducted using rabbit anti-PTEN (Abcam, Cambridge, MA, USA; 1:4,000), mouse anti-P53 (Novus Biologicals, Littleton, CO, USA; 1:1,000), mouse anti-FLAG (1:1,000), rabbit anti-P21 (Cell signaling, Danvers, MA, USA; 1:1,000), rabbit anti-P27 (Cell Signaling, Danvers, MA, USA; 1:1,000), and mouse anti-β-actin (Sigma-Aldrich, St. Louis, MO, USA; 1:1,000).

2.9. Western blotting, immunohistochemistry and immunofluorescent staining

Cultured cells, human BC specimens or xenotransplanted mouse tumor tissues were homogenized in a Polytron homogenizer in an SDS-lysis buffer (10% SDS, 20 mM Tris/HCl (pH 7.4), 50 mM NaCl, 5 mM β-mercaptoethanol and a mixture of protease inhibitors). The total proteins (10 μg) were resolved on 15% SDS-PAGE and transferred onto polyvinylidene fluoride (PVDF)-Immobilon membrane. After blocking with 5% milk in PBS, the membrane was incubated first with primary antibodies and then corresponding secondary antibodies conjugated with peroxidase. The primary antibodies and their working dilutions were: anti-PTEN (1:4,000); anti-phospho-PTEN (Ser370, 1:500), anti-phospho-PTEN (Ser380, 1:1,000), anti-phospho-PTEN (Ser385, 1:500), anti-AKT (1:1,000), anti-phospho-AKT (Thr308, 1:1,000), anti-phospho-AKT (Ser473, 1:1,000), anti-mTOR (mTOR, 1:1,000), anti-phospho-mTOR (Ser2448, 1:500), anti-phospho-S6 kinase (Ser235/236, 1:1,000), anti-TSC2 (1:1,000), anti-phospho-TSC2 (Ser939, 1:500), anti-phospho-TSC2 (Thr1462, 1:1,000), anti-MAPK (1:1,000), and anti-β-actin (1:3,000). All the antibodies were purchased from Cell Signaling Technology (Danvers, MA, USA), except anti-PTEN (from Abcam, Cambridge, UK), anti-phospho-PTEN (Ser385; from EMD Millipore, Burlington, MA, USA), and anti-β-actin (from Sigma-Aldrich, St. Louis, MO, USA).

For immunohistochemical and immunofluorescence staining, 5-μm thick sections were cut, deparaffinized and rehydrated and underwent antigen unmasking in citrate buffer (pH 6.0) via microwaving at the maximum power for 20 min. The sections were incubated with anti-KRT5 (Cell Signaling, Danvers, MA, USA; 1:200), anti-phosphor-MAPK (Cell Signaling, Danvers, MA, USA; 1:100), anti-Ki67 (Abcam, Cambridge, UK; 1:500), anti-KRT6B (ThermoFisher, Waltham, MA, USA; 1:250), anti-KRT13 (Abcam, 1:200), anti-KRT20

Author Manuscript Author Manuscript Author Manuscript Author Manuscript

(Origene, Rockville, MD, USA; 1:100), and anti-MCM2 (Abcam, Cambridge, UK 1:200), followed by corresponding secondary antibodies conjugated with either peroxidase (for immunohistochemistry) or fluorescein (for immunofluorescence). Ki-67-positive cells were enumerated at 100 x magnification on five sections per bladder from three mice per group, averaged and expressed as the number of positive cells per section per mouse. For the assessment of the subcellular localization of PTEN, UMUC3 cells stably transfected with full-length PTEN were cultured in 0, 2, and 10% FBS for 24 h. The cells were permeabilized with pre-cooled acetone/methanol (1:1) and stained with anti-PTEN followed by rhodamine-conjugated secondary antibody and immunofluorescent microscopy.

2. 10. Xenograft mouse model

Athymic male nude mice (CrTac:NCr-Foxn1nu; sp/sp) were purchased from Taconic Biosciences (Hudson, New York, USA) and randomized into three groups (n=15). UMUC3 cells stably transfected with (i) CMV-rtTA; (ii) CMV-rtTA / Tre-full length PTEN; or (iii) CMV-rtTA / Tre-tailless PTEN were injected subcutaneously (1×10^6 cells/per site) into the lower back of the mice. The mice were placed on a regular diet for seven days before half of the mice within each of the aforementioned three groups started to receive a diet containing doxycycline (20 g/Kg body weight). The regular or doxycycline diet continued for additional two weeks after which all the mice were euthanized and their tumors were weighed and subjected to further analysis.

2. 11. Intravesicle delivery of tailless PTEN in transgenic mice

The cDNA encoding full-length or tailless *Pten* was cloned into pUAS-Luc2 (Addgene #24343; Watertown, MA, USA) to construct EF1a-*Pten*-SV40 polyA or EF1a-tailless *Pten*-SV40 polyA. Each expression cassette was ligated into pAdenoX vector, sequence-verified and transfected into Adeno-X 293 cells. The adenoviruses were isolated using the freeze-thawing methods, and high-titer stocks were prepared by amplifying the primary stock in 293 cells.

For intravesicle delivery, 3-month-old female *Upk2-HRas*$^{*/*}$ transgenic mice [29] were anesthetized with Ketamine/Xylazine, and a 24-gauge catheter was introduced into the bladder via the urethra. The bladder was washed with 100 μL PBS, then with 100 μL 0.1% n-dodecyl-α-D-maltoside (DDM; Sigma-Aldrich, St. Louis, MO, USA) in PBS three times, and then administered with 100 μL adenovirus reconstituted in PBS containing 0.05% DDM (approximately 1,010 IFU/mL). The viral solution was retained in the bladder for 1 h, and the mice were permitted to recover from anesthesia. The instillation was done once a week for three weeks after which all the mice were euthanized. The bladders were weighed, and the bladder volume was calculated with formula V=(L x *W x *D)/2.

2. 11. Statistical Analysis

Two-tailed, student's *t* tests were used to assess the statistical differences. *A P* value <0.05 was considered statistically significant.

Author Manuscript Author Manuscript Author Manuscript Author Manuscript

3. Results

3.1. Time-controlled ablation of Tp53 or Pten in adult mouse urothelial cells leads to minimal pathological alterations

To ascertain the functional relationship between the RTK-RAS-PI3K and P19-P53-P21 pathways in the genesis of MIBC and its molecular subtype, we chose to ablate *Pten* and *Tp53*, alone or in combination, using a urothelium-specific and time-controlled knockout system that we previously developed. The system comprised of a transgenic line in which a 3.6-kB murine uroplakin 2 (*Upk2*) promoter controlled the expression of a reverse tetracycline transactivator version M2 (*rtTA-M2*) [24, 25] and another transgenic line in which tetracycline response elements drove the expression of Cre recombinase (*Tre-Cre*; Fig. 1A). *Cre* was only expressed when double transgenic mice bearing both transgenes (e.g., *mUpk2-rtTA-M2* / *Tre-Cre*) were exposed to doxycycline which bound to and activated *rtTA-M2* in a conformation-dependent manner (Fig. 1A). Upon cross-breeding between the aforementioned double transgenic mice and floxed *Tp53* mice in which exons 5 and 6 (encoding the DNA-binding domain) of *Tp53* gene were flanked by two loxP sites ($Tp53^{fl}$) and further intercrosses among the offspring, we obtained mice bearing *mUpk2-rtTA-M2* / *Tre-Cre* / $Tp53^{fl/fl}$ (abbreviated as $Tp53^{fl/fl}$ from here on). An identical breeding strategy was used to obtain *mUpk2-rtTA-M2* / *Tre-Cre* / $Pten^{fl/fl}$ (abbreviated as $Pten^{fl/fl}$ from here on). When mice of both genders reached adulthood (2-3 months of age), their regular food pellets were switched to those supplemented with 20 g/kg doxycycline and fed *ad libitum* continuously until they were euthanized..

After three months of doxycycline treatment (six months of age), the total urothelial proteins were subjected to western blotting (Fig. 1B). P53, which was present in the WT, was not detected in $Tp53^{fl/fl}$ mice; this was accompanied by a marked reduction of P53 downstream effector P21 (Fig. 1B). PTEN, which was also present in the WT mice, was not detectable in the $Pten^{fl/fl}$ mice (Fig. 1B). The loss of PTEN was accompanied by increased levels of activated (phosphorylated) AKT (at residue 473; Fig. 1B and 1C), which is consistent with the fact that PTEN is normally a potent inhibitor of AKT phosphorylation/activation. Histologically, $Tp53^{fl/fl}$ mice exhibited normal urothelial morphology, whereas $Pten^{fl/fl}$ mice exhibited mild hyperplasia with increased urothelial layers (from 2-3 layers to 4-5 layers) and expression of phosphorylated MAPK (Fig. 1C), which was consistent with Fig. 1B. In comparison, no significant increase in the expansion of KRT5-positive, urothelial basal cells in $Pten^{fl/fl}$ mice was observed (Fig. 1C, lower row/right panel), suggesting that the urothelial proliferative rate at the steady state in these $Pten^{fl/fl}$ mice was relatively limited.

3.2. Loss of both alleles of both Tp53 and Pten in adult mouse urothelial cells triggers basal/squamous MIBC

Being unable to observe a tumor in mice lacking *Tp53* or *Pten*, we next tested whether the two events together would cooperate leading to urothelial tumorigenesis, by intercrossing the above-described $Tp53^{fl/fl}$ and $Pten^{fl/fl}$ mice. Figure 2A was a representative cohort after several crosses, and of the multiple genotypes, we first focused on *mUpk2-rtTA-M2* / *Tre-Cre*/ $Tp53^{fl/fl}$ / $Pten^{fl/fl}$ mice. Adult (2-3 months old) male and female mice were fed with doxycycline-containing food *ad libitum* continuously for three or five months (mouse aged

Author Manuscript Author Manuscript Author Manuscript Author Manuscript

six or eight months) at which point they were euthanized. By histopathological examination, 5/5 of the 6-month-old mice and 11/11 of the 8-month-old mice all developed MIBC (Fig. 2B; Table 1), with no observable age-related differences in pathological stage and grade. The invasive cells were strongly and uniformly positive for urothelial basal cell marker KRT5 (Fig. 2B), compared to normal urothelium which was confined to the bladder mucosa in the wild-type (WT) mice. Regions exhibiting squamous features were evident in all the *Tp53*$^{fl/fl}$ / *Pten*$^{fl/fl}$ mice examined (Fig. 2C). As expected, the invasive lesions were evidently labeled with antibodies against squamous differentiation markers, KRT6B [10] and KRT13 [30, 31], by immunofluorescent microscopy (Fig. 3; Supplementary Figs. 2 and 3). These proteins were completely absent in normal mouse urothelial cells from the wild-type mice (Supplementary Figs. 4 and 5). While the MIBC phenotype in mice lacking both *Tp53* and *Pten* was 100% penetrant, only normal urothelium and mild urothelial hyperplasia were observed in *Upk2-rtTA-M2* / *Tre-Cre* / *Pten*$^{fl/WT}$ / *Tp53*$^{fl/fl}$ and *Upk2-rtTA-M2* / *TRE-Cre* / *Pten*$^{fl/fl}$ / *Tp53*$^{fl/WT}$, respectively (Supplementary Fig. 1). These results strongly suggest that the complete loss of both *Tp53* and *Pten* is necessary to trigger basal/squamous MIBC.

3.3. Phosphorylation of the C-terminus of PTEN is highly prevalent in human BC cell lines and specimens

Although deletion and mutation of *Tp53* affects approximately 50% of human MIBC, those of *Pten* occur in 0-6% of the cases [16, 18, 19], raising the possibility that *Pten* is inactivated mainly by other mechanisms. Hyper-phosphorylation of PTEN at the C-terminus, which was detected in cultured tumor cells of non-urothelial origins, is associated with reduced anti-proliferative/tumor-suppressive activities of PTEN [32]. To test whether this was true in BC, we use western blotting on a panel of cell lines derived from and representing different grades and stages of human BC including RT4 (grade-1, non-invasive), RT112 (grade-2, invasive), 5637 (grade-2, invasive), 1376 (grade-3, invasive), TCCsup (grade-4, anaplastic, metastatic), T24 (grade-3, invasive), J82 (grade-3, invasive) and SCaBER (invasive, squamous cell carcinoma; Fig. 4A). The antibody against total PTEN detected the protein in all the cell lines except one (J82). J82, like another BC cell line, UMUC3 (see later), was known to exhibit homozygous deletion of the *Pten* locus [33, 34]. Interestingly, in all the other cell lines that expressed PTEN, the protein was uniformly phosphorylated at the C-terminus, as evidenced by the strong reactivity to phosphorylation-site-specific antibodies (PTEN-S370 and PTEN-S380; Fig. 4A). PTEN in T24, a cell line known to express a mutated PTEN [33, 34], was also C-terminally phosphorylated, suggesting the inactivation of one PTEN gene allele by mutation and the functional inactivation of the protein product of the second PTEN allele.

To examine the *in vivo* relevance of the above observations, we conducted western blotting of PTEN and phosphorylated PTEN on a cohort of freshly frozen, low- (T1-T7) and high- (T8-T14) grade, non-invasive bladder tumors (Fig. 4B). When PTEN was phosphorylated at S380, other phosphorylated sites of the C-terminus, such as S370, were also phosphorylated (Fig. 4A; and unpublished data), therefore we focused on PTEN-S380 here on unless otherwise noted. Of the 14 tumors examined, T5 and T9 had degraded proteins, as evidenced by the lack of detectable internal control MAPK. T4 and T7 were devoid of PTEN, likely

Author Manuscript Author Manuscript Author Manuscript Author Manuscript

due to homozygous PTEN deletion. The rest of the 10 tumors, however, had detectable PTEN. Importantly, whenever PTEN was detected, it was phosphorylated (Fig. 4B).

3.4. Functional effects of C-terminal phosphorylation of PTEN on down-stream signaling and BC cell survival

To determine the cellular effects of PTEN's C-terminal phosphorylation on BC cells, we performed site-directed mutagenesis replacing one or more of the six potential phosphorylation sites (T366, S370, S380, T382, T383 and S385) with phosphorylation-incompatible alanine(s). These mutants, along with a mock vector-only control and a WT PTEN control, were separately transiently transfected into UMUC3 cells that lacked endogenous PTEN. The expression of a WT PTEN reduced AKT activation (phosphorylation at S473), compared with non-transfected or mock vector-transfected controls (Fig. 4C; compare lane 3 with lanes 1 and 2). Nevertheless, the exogenously expressed PTEN was phosphorylated at both S380 and S385 (Fig. 4C; top two panels, lane 3). Replacing the two serines with alanines abolished the phosphorylation at these two sites (Fig. 4C; lanes 4 and 5); and this was accompanied by a reduced AKT activation/phosphorylation (Fig. 4C; compare lanes 4 and 5 with lane 3), and a corresponding decrease in cell survival (Fig. 4E; compare columns 4 and 5 with column 3). Interestingly, mutating one phosphorylation site (e.g., S380) negatively affected the phosphorylation of another site (e.g., S385) - an effect that was reciprocal (Fig. 4C; lanes 4 and 5). Increasing the mutation sites at the C-terminus to two (S380 and S385 simultaneously), four (S380, T382, T383 and S385) and six (T366, S370, S380, T382, T383 and S385), however, did not have additional inhibitory effects on AKT activation/phosphorylation (compare lanes 6-8 with lanes 4 and 5). These results suggest that the C-terminal phosphorylation at different residues is a highly coordinated event and may proceed via different cascades with the initial phosphorylation site and its kinase playing major roles in determining whether the subsequent sites are phosphorylated [35]. Our results also suggest that detection of phosphorylation at one site may be a reasonable surrogate for the phosphorylation status of the entire C-terminus of PTEN.

To complement the phosphorylation-depleting experiments, we replaced, using similar site-directed mutagenesis, serine/threonine residues within PTEN's C-terminus with negatively charged aspartate(s) singly or in various combinations (Fig. 4D). These phosphorylation-mimicking mutants were less potent than the WT PTEN in inhibiting AKT activation/phosphorylation and cell survival (Fig. 4D; compare lanes 4-8 with lane 3; and Fig. 4F, compare columns 4-8 with column 3). The additional number of sites of phosphorylation-mimicking mutations again did not have an added effect on the loss of PTEN's overall inhibitory activity on AKT (Fig. 4F; compare lanes from 4-8). The biological differences between the mutated versions of PTEN (both phosphorylation-depleting and phosphorylation-mimicking) and the WT PTEN were considered significant, given the fact that not all the cells were transfected in these transient transfection experiments.

Author Manuscript Author Manuscript Author Manuscript Author Manuscript

3.5. Effects of full-length and tailless PTEN on BC cell survival and signaling are dependent on growth conditions

The fact that the inhibitory effects of PTEN on AKT and cell survival could be negated by the C-terminal phosphorylation of PTEN prompted us to systematically compare full-length with tailless PTEN under different culture conditions. We stably transfected PTEN-lacking UMUC3 cells and PTEN-mutation-expressing T24 cells with a mock vector, full-length PTEN, or tailless PTEN with deletion of the C-terminus after residue 352 (Fig. 5A and B). Stably transfected cells were then grown in culture media containing 0, 2, or 10% FBS. In 0% (serum-free) media, the growth of both UMUC3 and T24 were curtailed, and the expression of either full-length or tailless PTEN further reduced the cell growth to comparable levels at 24 and 48 h (Fig. 5A and B). At 2% FBS, the cell growth of mock vector transfected cells accelerated significantly, particularly at 48 h. However, both full-length and tailless PTEN were equally effective in restraining cell growth to the base level. At 10% FBS, however, the growth-inhibitory effects by the full-length PTEN were significantly compromised. While the full-length PTEN failed to inhibit cell growth at 10% FBS, the tailless PTEN remained highly potent as a growth inhibitor (Fig. 5A and B) in both BC cell lines. Western blotting showed that phosphorylation of the full-length PTEN was significantly higher in 10% than in 0 and 2% FBS (Fig. 5C). This corresponded well with the level of AKT phosphorylation that is comparable to mock-transfected control in 10% FBS, thus establishing C-terminal phosphorylation and functional inactivation of full-length PTEN in high-serum media. In contrast, tailless PTEN-transfected cells had markedly reduced cell survival and reduced AKT activation even in the presence of 10% FBS (Fig. 5C). Importantly, these divergent effects of full-length and tailless PTEN under different culture conditions were highly reproducible with both UMUC3 and T24 cells, the latter of which contained an endogenous mutated PTEN (Fig. 5B and D). Utilizing immunofluorescent staining, it was apparent that the full-length PTEN had a greater plasma membrane association in serum-free medium than that in serum-containing media (Fig. 5E). This supports the idea that the phosphorylation of PTEN drives it into the cytoplasm, making it less active.

3.6. Divergent tumor-suppressive effects of full-length and tailless PTEN on BC cells

As PTEN is known to affect PI3K-independent signaling pathways particularly in regards to its ability to bind and activate p53 [28] and because PTEN and p53 deficiency collaborates in mice to induce MIBC (Figs. 1 and 2; Table 1; Ref. [15]), we examined whether tailless PTEN differed from full-length PTEN in binding to and activating p53. To this end, we conducted co-immunoprecipitation (IP) using UMUC3 cells double-transfected with FLAG-tagged WT p53 along with tailless or full-length PTEN (Supplementary Fig. 6A). Both IP and reverse IP showed markedly higher binding between tailless PTEN and p53. Consistent with this, the levels of p21 and p27, transcriptional targets of p53 [36], were higher in UMUC3 expressing tailless PTEN than those expressing full-length PTEN (Supplementary Fig. 6B).

To gain a deeper understanding of the impact of the C-terminal phosphorylation of PTEN on tumorigenesis, we compared the effects of expressing full-length versus tailless PTEN on apoptosis, cell-cycle progression, cell migration and invasion of UMUC3 cells

Author Manuscript Author Manuscript Author Manuscript Author Manuscript

(Supplementary Fig. 6C-6F). While the full-length and tailless PTEN both triggered about a 5-fold increase of apoptosis over mock vector-transfected cells in serum-free medium, this pro-apoptotic effect was significantly blunted with the full-length PTEN in 2% FBS and completely abolished in 10% FBS, but this was not noted with the tailless PTEN (Supplementary Fig. 6C). In this high-serum medium, the full-length PTEN-transfected cells had less partition in G0/G1 phase than that of the tailless PTEN-transfected cells (Supplementary Fig. 6D). Similarly, cell migration (inversely related to the remaining gaps) and invasion were significantly higher in the full-length PTEN-transfected cells in high-serum medium than those in the tailless PTEN-transfected cells (Supplementary Fig. 6E and 6F). These data add additional support from a functional perspective to the idea that the full-length PTEN can be disabled in the presence of abundant growth factors and that the tailless PTEN, which cannot be phosphorylated at the C-terminus, is a more potent tumor suppressor.

3.7. Effects of inducible expression of full-length PTEN and tailless PTEN in vitro and in vivo

A major technical hurdle that we encountered during our transfection experiments was the difficulty to maintain and passage stably transfected cells by the tailless PTEN due to its severe cytotoxic effects. To circumvent this challenge and prepare for *in vivo* animal experiments, we established an inducible expression system by first stably transfecting UMUC3 cells with CMV-driven reverse tetracycline transactivator (CMV-rtTA) and then by stably transfecting these cells with tetracycline response element (TRE)-driven full-length or tailless PTEN. Expression of the full-length or the tailless PTEN was then induced acutely by exposing double-stably transfected cells to the doxycycline inducer. As with the constitutive expression, the inducible expression of the tailless PTEN exerted greater inhibitory effects on AKT phosphorylation than that of the inducible expression of the full-length PTEN, particularly in high-serum media (Supplementary Fig. 7A and 7C). Similar inhibitory effects by the tailless PTEN were observed with additional down-stream effectors of the PTEN-PI3K signaling pathway including the phosphorylation of TSC2, mTOR, and S6 (Supplementary Fig. 7B).

We next assessed the inhibitory effects of the full-length and tailless PTEN on tumor growth *in vivo* using a xenograft mouse model. UMUC3 bearing stably transfected (i) CMV-rtTA alone, (ii) CMV-rtTA and TRE-full-length PTEN, or (iii) CMV-rtTA and TRE-tailless PTEN were injected subcutaneously into athymic nude mice. The tumor cells were allowed to grow for seven days until tumors were visible in all mice before they were fed with doxycycline-containing food to induce gene expression. No significant difference in tumor size and weight was observed in UMUC3 cells bearing CMV-rtTA and TRE-full-length PTEN before and after doxycycline induction, neither was there difference between these two groups and those bearing CMV-rtTA alone (Fig. 6A and 6B). This suggests that the full-length PTEN was ineffective in inhibiting tumor growth. In contrast, UMUC3 cells bearing CMV-rtTA and TRE-tailless PTEN had markedly reduced ability to further develop into the tumors after doxycycline treatment, compared to that in the un-induced group or induced full-length PTEN group (Fig. 6A and 6B). Western blotting of residual tumor masses showed that the full-length PTEN was phosphorylated at the C-terminus, had reduced inhibitory effects

Author Manuscript Author Manuscript Author Manuscript Author Manuscript

on AKT, TSC2, mTOR and S6 phosphorylation (Fig. 6C), and Ki67 expression (Fig. 6D and 6E), compared with the tailless PTEN. There was a small amount of PTEN detected in the (No PTEN) controls (Fig. 6C), which likely originated from the non-tumor matrix cells from the mouse hosts that had grown into the tumor masses; these endogenous mouse PTEN molecules were not phosphorylated at the C-terminus. Interestingly, P-AKT-S473 was slighter higher in the PTEN-FL group than in the No PTEN group. The reason for this is unclear, but it could be due to serine/threonine kinases whose activities are not controlled by full-length PTEN. These kinases could be upregulated in BC cells *in vivo*. Xenograft tumor cells expressing the tailless PTEN also expressed much less proliferation marker MCM2 than control tumor cells expressing no tailless PTEN (Fig. 6F). Altogether, our results indicated that the full-length PTEN could be functionally inactivated by C-terminal phosphorylation and the tailless PTEN is a more potent tumor suppressor than the full-length PTEN *in vivo*.

3.8. Intravesicle delivery of tailless PTEN inhibits bladder tumor growth in transgenic mice

To evaluate the tumor-inhibitory effects of tailless PTEN *in situ*, we took advantage of our *Upk2-HRas*$^{*/*}$ transgenic mice which developed early-onset non-muscle-invasive bladder tumors [29]. Adenovirus-driven tailless PTEN and control full-length PTEN were introduced separately via the transurethral route into the bladders of 3-month-old female transgenic mice once a week for three weeks. Upon mouse euthanization, we noted a significant reduction of bladder volume and weights in tailless PTEN-treated mice, compared to those in the full-length PTEN-treated mice (Fig. 7A). During histological examination, the Vector-treated mice exhibited multifocal bladder tumors, whereas the full-length PTEN-treated mice had nodular hyperplasia and occasional bladder tumors (Fig. 7B). In contrast, the tailless PTEN treated mice exhibited primarily simple urothelial hyperplasia that expressed considerably lower levels of MCM2 than the tumor lesions of the Vector- and full-length PTEN-treated mice (Fig. 7B). Thus, the tailless PTEN is more potent in inhibiting tumor growth when delivered intravesically.

4. Discussion

We demonstrated here that, although time-controlled ablation of either *Tp53* or *Pten* in adult mouse urothelial cells elicited minimal amounts of morphological changes, normal urothelium in the case of *Tp53* ablation and urothelial hyperplasia in the case of *Pten* ablation; Table 1; Supplementary Fig. 1), ablation of both genes is sufficient to fully initiate the formation of MIBC (Table 1; Fig. 2). We showed that MIBC in mice lacking *Tp53* and *Pten* displayed morphological features and expressed markers that were typical of basal/squamous subtype of MIBC (Figs. 2 and 3). These results echo our earlier observation in mice expressing a mutationally activated *HRas* and lacking *Tp53* in urothelial cells, as this genetic combination also led to the formation of basal/squamous subtype MIBC [27]. Our consistent results from these two mouse models underscore the notion that the inactivation of PTEN, which leads to the over-activation of PI3K, is functionally equivalent to RAS activation which also activates PI3K. Our results reinforce the close collaborative relationship between RTK-RAS-PI3K and P19-P53-P21 pathway alterations, both of which

Author Manuscript Author Manuscript Author Manuscript Author Manuscript

are highly prevalent in human MIBC [10], in the tumorigenesis of MIBC, especially the basal/squamous subtype of MIBC.

A notable difference between *Pten* ablation and *HRas* activation in the context of *Tp53* deficiency is the onset and penetrance of MIBC. Under the condition of *HRas*-activation and *Tp53*-null, MIBC arises in about 10% of the mice by six months of age and then in 60% of the mice by 16-months of age [27]. Under the condition of *Pten-null* and *Tp53*-null, MIBC forms in 100% of the mice by six months of age (Table 1). This occurs despite the fact that activated *HRas* by itself is considerably more pro-proliferative in inducing widespread urothelial hyperplasia in all mice by two months of age [29, 37] than *Pten* loss alone, which is associated with only sporadic urothelial hyperplasia primarily in aged mice (Supplementary Fig. 1; [38, 39]). It therefore appears that PTEN loss collaborates with P53 loss in a manner that is not totally dependent on the proliferative effects of PTEN loss. Instead, other mechanisms may be at play (see later in this work). This type of varied tumorgenicity between P53 loss and RTK-RAS-PI3K pathway may be extended to other factors in this pathway. Of particular interest is FGFR3 which is frequently activated by mutation, gene fusion and overexpression in human MIBC [10]. Thus far, expression of several activating FGFR3 mutants, located in the extracellular loop domain or the intracellular kinase domain, in mouse urothelium leads to normal-appearing urothelium without apparent hyperplasia or tumor formation [40, 41]. Crossing FGFR3 mutant mice with SV40T mice leads to the development of high-grade non-invasive BC (e.g., pTaG2-3) [42]. Since SV40T-mediated inactivation of P53 is incomplete [43], it will be interesting to see whether the total loss of P53 collaborates with mutated FGFR3 to trigger MIBC and, if so, whether such MIBC belongs to the luminal subtype as suggested by clinical correlative studies. Similarly, it would be interesting to determine whether FGFR3 gene fusion or overexpression collaborates with P53 deficiency to induce MIBC and its subtypes.

Another notable observation in this study is that the deletion of two alleles of *Tp53* plus the deletion of one allele of *Pten* resulted in normal urothelium, whereas the deletion of two *Pten* alleles plus the deletion of one *Tp53* allele led to urothelial hyperplasia (Table 1; Supplementary Fig. 1). Thus, mono-allelic deletion of either *Tp53* or *Pten* did not exacerbate the phenotype caused by the biallelic deletion of its collaborative partner. In other words, tumorigenesis of MIBC commenced only when both alleles of both *Tp53* and *Pten* genes were deleted (Table 1). While concurrent mutation of one *Tp53* allele and loss of the contralateral allele, rendering P53 completely non-functional [44], is common in human MIBC, mutation or deletion of *Pten* is extremely rare in human MIBC [16, 18, 19]. This high degree of imbalance in the frequencies of genetic alterations between *Tp53* and *Pten* could indicate that *Pten* defects are unimportant in MIBC tumorigenesis. However, it could also indicaten that PTEN is inactivated on a protein level by modifications other than mutation or deletion. The latter reasoning prompted us to examine the expression status of PTEN in human BC cell lines and specimens, and whether PTEN could be functionally inactivated in MIBC – questions that have thus far received minimal attention.

Western blotting indicated that PTEN was expressed in a majority of human BC cell lines and patient specimens (Fig. 4A and 4B). This result is opposite to several previous immunohistochemical studies showing reduced expression of PTEN in human BC [38, 45],

Author Manuscript Author Manuscript Author Manuscript Author Manuscript

but is in strong agreement with the data published by the Netto group [20] and Koksal et al. [46], indicating continued or even increased PTEN expression in human BC. It is possible that the differences in antigen preservation, antibody affinity and specificity, and sources, and inclusion or exclusion of normal controls underlie these divergent results on PTEN expression.

In addition to demonstrating the overexpression of PTEN in human BC, we further showed that PTEN is hyper-phosphorylated at the C-terminus in all the cases in which PTEN is expressed. To the best of our knowledge this is the first time C-terminal phosphorylation of PTEN was evaluated in human BC specimens. The role of C-terminal phosphorylation of PTEN in functionally disabling PTEN was supported by our site-directed mutagenesis experiments, in which the loss of the C-terminal phosphorylation sites increased PTEN's growth inhibitory activity (Fig. 4A and 4A'), whereas the constitutive phosphorylation-mimics decrease PTEN's activity (Fig. 4B and 4B'). By demonstrating the functional inactivation of PTEN, our resultsprovide a missing link between the very low frequency of genomic alterations of PTEN in human BC [10, 14, 16, 18, 19, 38], and PTEN as a co-tumor-driver with p53 deletion in genetically engineered mice [15]. Therefore, instead of a deleted or mutated PTEN to collaborate with p53 deficiency to drive MIBC, it is more likely that phosphorylated, dysfunctional PTEN drives these tumors in collaboration with p53 defects. In this regard, phosphorylated PTEN, rather than total PTEN, along with p53, should be used in the biomarker panel for tumor subtyping, risk stratification and prognosis prediction for human BC. Additional retrospective studies with outcome information and prospective studies are required to further establish the utility of this biomarker combination.

From a mechanistic standpoint, the hyper-phosphorylation of the C-terminus of PTEN in BC cells may exert several major effects on PTEN's overall conformational structure similar to those observed in cell-free systems and in cultured non-BC cells. For example, the hyper-phosphorylated, highly negatively charged C-terminus has been shown to interact with the positively charged C2-domain of PTEN, structurally changing PTEN from an enzymatically active "open" conformation to an inactive "closed" conformation [47-51]. The phosphorylation-induced "closed" conformation of PTEN tends to be more cytoplasmic and stable, as was shown in BC cells (Fig. 5C), making PTEN less active in its membrane-dependent lipid phosphatase against PI3K [51-53]. The hyper-phosphorylated PTEN C-terminus has been shown to interact with the phosphatase domain, thus directly impairing its activity. In addition to the PTEN-related functions, the C2-domain of PTEN can bind to and activate p53. Shielding of the C2-domain by a hyper-phosphorylated C-terminus would likely disrupt the binding and activation of p53 [28]. This is indeed the case as demonstrated in this study using tailless PTEN which leaves the C2 domain in an open position, allowing it to bind significantly more p53 than that by the full-length PTEN (Supplementary Fig. 6A). The combined effects of tailless PTEN on enhancing its phosphatase activity and p53 binding likely explain why the tailless PTEN is considerably more potent than the full-length PTEN in inhibiting cell proliferation, cell-cycle progression, migration, *in vitro* invasion (Fig. 5; Supplementary Figs. 6 and 7), and *in vivo* tumor growth (Figs. 6 and 7).

Our data, particularly those demonstrating the potency of the tailless PTEN as a growth inhibitor/tumor suppressor, may have therapeutic implications. As shown in the BC cell

Author Manuscript Author Manuscript Author Manuscript Author Manuscript

lines, the tailless PTEN markedly reduced cell survival in cells lacking PTEN or bearing a PTEN mutation (Fig. 5; Supplementary Fig. 7). The tailless PTEN also substantially suppressed cell migration and invasion and induced apoptosis and cell-cycle progression (Supplementary Fig. 6). Based on these activities, the tailless PTEN will likely be an effective inhibitor of BC harboring mutations and/or deletions of PTEN. The tailless PTEN should also be effective for the majority of BC that express a WT PTEN but is functionally inactivated by C-terminal phosphorylation, because the tailless PTEN cannot be phosphorylated and remains functionally active even in the presence of abundant growth factors (Figs. 5-7; Supplementary Fig. 7). Since BC is readily accessible via the transurethral route, it is possible to deliver the tailless PTEN locally via viral vectors or nanoparticles. The tailless PTEN could also be used to enhance the efficacy of conventional chemotherapeutics and/or immune modulators already in use or in clinical trials.

Supplementary Material

Refer to Web version on PubMed Central for supplementary material.

Acknowledgments

This work was supported in part by grants from the United States National Institutes of Health (P01 CA165980 and R01DK110466) and Veterans Affairs Office of Research and Development (Biomedical Laboratory Research and Development Service, Merit Review Awards (I01BX002049 and 1I01BX005602) and Research Career Scientist Award (IK6BX004479) to XRW).

Abbreviations

PTEN	Phosphatase and Tensin Homolog
MIBC	Muscle-invasive bladder cancer
RTK	Receptor Tyrosine Kinase
PI3K	Phosphoinositide 3-kinase
KRT20	Cytokeratin 20
GATA3	GATA Binding Protein 3
FOXA1	Forkhead Box A1
KRT5	Cytokeratin 5
KRT14	Cytokeratin 14
KRT6	Cytokeratin 6
DSC3	Desmocollin 3
SOX2	SRY-Box Transcription Factor 2
DLX6	Distal-Less Homeobox 6
PD-L1	Programmed Death-ligand 1

Author Manuscript Author Manuscript Author Manuscript Author Manuscript

CLTA-4	Cytotoxic T-Lymphocyte Associated Protein 4
PD-L1	Programmed Cell Death Protein 1
Cre	Cre recombinase FGFR3
MCM2	minichromosome maintenance complex component 2
rtTA	reverse tetracycline transactivator
Tre	tetracycline response element
FVB/N	Friend Virus B /N mouse strain
FBS	fetal bovine serum
PBS	phosphate-buffered saline
SDS-PAGE	sodium dodecyl-sulfate polyacrylamide gel electrophoresis
PVDF	polyvinylidene fluoride
KRT13	Cytokeratin 13
CMV	Cytomegalovirus
DDM	n-dodecyl-α-D-maltoside
Upk2	Uroplakin 2
MAPK	Mitogen-Activated Protein Kinase
AKT	AKT Serine/Threonine Kinase 1
TSC2	Tuberous Sclerosis Complex 2
mTOR	Mammalian Target of Rapamycin
S6	Ribosomal protein S6
Fibroblast	growth factor receptor 3

References

[1]. Werntz RP, Smith ZL, Packiam VT, Smith N, Steinberg GD, The Impact of Lymphovascular Invasion on Risk of Upstaging and Lymph Node Metastasis at the Time of Radical Cystectomy, Eur. Urol. Focus 6 (2020) 292–297. [PubMed: 30297221]

[2]. Knowles MA, Hurst CD, Molecular biology of bladder cancer: new insights into pathogenesis and clinical diversity, Nat. Rev. Cancer 15 (2015) 25–41. [PubMed: 25533674]

[3]. Shah JB, McConkey DJ, Dinney CP, New strategies in muscle-invasive bladder cancer: on the road to personalized medicine, Clin. Cancer Res 17 (2011) 2608–2612. [PubMed: 21415213]

[4]. Kamat AM, Hahn NM, Efstathiou JA, Lerner SP, Malmstrom PU, Choi W, Guo CC, Lotan Y, Kassouf W, Bladder cancer, Lancet. 388 (2016) 2796–2810. [PubMed: 27345655]

[5]. Lokeshwar SD, Lopez M, Sarcan S, Aguilar K, Morera DS, Shaheen DM, Lokeshwar BL, Lokeshwar VB, Molecular Oncology of Bladder Cancer from Inception to Modern Perspective, Cancers (Basel). 14 (2022) 14:2578. [PubMed: 35681556]

Author Manuscript Author Manuscript Author Manuscript Author Manuscript

[6]. Parekh DJ, Bochner BH, Dalbagni G, Superficial and muscle-invasive bladder cancer: principles of management for outcomes assessments, J. Clin. Oncol 24 (2006) 5519–5527. [PubMed: 17158537]

[7]. Stamatakis L, Godoy G, Lerner SP, Innovations in radical cystectomy and pelvic lymph node dissection, Semin Oncol. 39 (2012) 573–582. [PubMed: 23040253]

[8]. American Cancer Society. Cancer Facts and Figures 2022. Atlanta, GA, American Cancer Society. (2022).

[9]. Wu XR, Urothelial tumorigenesis: a tale of divergent pathways, Nat. Rev. Cancer 5 (2005) 713–725. [PubMed: 16110317]

[10]. Robertson AG, Kim J, Al-Ahmadie H, Bellmunt J, Guo G, Cherniack AD, Hinoue T, Laird PW, Hoadley KA, Akbani R, et al. , Comprehensive Molecular Characterization of Muscle-Invasive Bladder Cancer, Cell. 171 (2017) 540–556.e525. [PubMed: 28988769]

[11]. Seiler R, Ashab HA, Erho N, van Rhijn BW, Winters B, Douglas J, Van Kessel KE, Fransen van de Putte EE, Sommerlad M, Wang NQ, e al., Impact of Molecular Subtypes in Muscle-invasive Bladder Cancer on Predicting Response and Survival after Neoadjuvant Chemotherapy, Eur. Urol 72 (2017) 544–554. [PubMed: 28390739]

[12]. Choi W, Porten S, Kim S, Willis D, Plimack ER, Hoffman-Censits J, Roth B, Cheng T, Tran M, Lee IL, et al., Cancer Cell. 25 (2014) 152–165. [PubMed: 24525232]

[13]. Gouin KH 3rd, Ing N, Plummer JT, Rosser CJ, Ben Cheikh B, Oh C, Chen SS, Chan KS, Furuya H, Tourtellotte WG, Knott SRV, Theodorescu D, An N-Cadherin 2 expressing epithelial cell subpopulation predicts response to surgery, chemotherapy and immunotherapy in bladder cancer, Nat. Commun 12 (2021) 4906. [PubMed: 34385456]

[14]. Network TCGA, Comprehensive molecular characterization of urothelial bladder carcinoma, Nature. 507 (2014) 315–322. [PubMed: 24476821]

[15]. Puzio-Kuter AM, Castillo-Martin M, Kinkade CW, Wang X, Shen TH, Matos T, Shen MM, Cordon-Cardo C, Abate-Shen C, Inactivation of p53 and Pten promotes invasive bladder cancer, Genes Dev. 23 (2009) 675–680. [PubMed: 19261747]

[16]. Aveyard JS, Skilleter A, Habuchi T, Knowles MA, Somatic mutation of PTEN in bladder carcinoma, Br. J. Cancer 80 (1999) 904–908. [PubMed: 10360673]

[17]. Sjodahl G, Lauss M, Gudjonsson S, Liedberg F, Hallden C, Chebil G, Mansson W, Hoglund M, Lindgren D, A systematic study of gene mutations in urothelial carcinoma; inactivating mutations in TSC2 and PIK3R1, PLoS One. 6 (2011) e18583. [PubMed: 21533174]

[18]. Cairns P, Evron E, Okami K, Halachmi N, Esteller M, Herman JG, Bose S, Wang SI, Parsons R, Sidransky D, Point mutation and homozygous deletion of PTEN/MMAC1 in primary bladder cancers, Oncogene. 16 (1998) 3215–3218. [PubMed: 9671402]

[19]. Liu J, Babaian DC, Liebert M, Steck PA, Kagan J, Inactivation of MMAC1 in bladder transitional-cell carcinoma cell lines and specimens, Mol. Carcinog 29 (2000) 143–150. [PubMed: 11108659]

[20]. Chaux A, Comperat E, Varinot J, Hicks J, Lecksell K, Solus J, Netto GJ, High levels of phosphatase and tensin homolog expression are associated with tumor progression, tumor recurrence, and systemic metastases in pT1 urothelial carcinoma of the bladder: a tissue microarray study of 156 patients treated by transurethral resection, Urology. 81 (2013) 116–122. [PubMed: 23273076]

[21]. Dempsey DR, Viennet T, Iwase R, Park E, Henriquez S, Chen Z, Jeliazkov JR, Palanski BA, Phan KL, Coote P, Gray JJ, Eck MJ, Arthanari H, Cole PA, The structural basis of PTEN regulation by multi-site phosphorylation, Nat. Struct. Mol. Biol 28 (2021) 858–868. [PubMed: 34625746]

[22]. Chen Z, Dempsey DR, Thomas SN, Hayward D, Bolduc DM, Cole PA, Molecular Features of Phosphatase and Tensin Homolog (PTEN) Regulation by C-terminal Phosphorylation, J. Biol. Chem 291 (2016) 14160–14169. [PubMed: 27226612]

[23]. Masson GR, Perisic O, Burke JE, Williams RL, The intrinsically disordered tails of PTEN and PTEN-L have distinct roles in regulating substrate specificity and membrane activity, Biochem. J 473 (2016) 135–144. [PubMed: 26527737]

Author Manuscript Author Manuscript Author Manuscript Author Manuscript

[24]. Zhou H, Liu Y, He F, Mo L, Sun TT, Wu XR, Temporally and spatially controllable gene expression and knockout in mouse urothelium, Am. J. Physiol. Renal Physiol 299 (2010) F387–395. [PubMed: 20427471]

[25]. Xia Y, Wang X, Liu Y, Shapiro E, Lepor H, Tang MS, Sun TT, Wu XR, PKM2 Is Essential for Bladder Cancer Growth and Maintenance, Cancer Res. 82 (2022) 571–585. [PubMed: 34903602]

[26]. Perl AK, Wert SE, Nagy A, Lobe CG, Whitsett JA, Early restriction of peripheral and proximal cell lineages during formation of the lung, Proc. Natl. Acad. Sci. USA 99 (2002) 10482–10487. [PubMed: 12145322]

[27]. He F, Melamed J, Tang MS, Huang C, Wu XR, Oncogenic HRAS Activates Epithelial-to-Mesenchymal Transition and Confers Stemness to p53-Deficient Urothelial Cells to Drive Muscle Invasion of Basal Subtype Carcinomas, Cancer Res. 75 (2015) 2017–2028. [PubMed: 25795707]

[28]. Freeman DJ, Li AG, Wei G, Li HH, Kertesz N, Lesche R, Whale AD, Martinez-Diaz H, Rozengurt N, Cardiff RD, Liu X, Wu H, PTEN tumor suppressor regulates p53 protein levels and activity through phosphatase-dependent and -independent mechanisms, Cancer Cell. 3 (2003) 117–130. [PubMed: 12620407]

[29]. Mo L, Zheng X, Huang HY, Shapiro E, Lepor H, Cordon-Cardo C, Sun TT, Wu XR, Hyperactivation of Ha-ras oncogene, but not Ink4a/Arf deficiency, triggers bladder tumorigenesis, J. Clin. Invest 117 (2007) 314–325. [PubMed: 17256055]

[30]. Aufderheide M, Ito S, Ishikawa S, Emura M, Metaplastic phenotype in human primary bronchiolar epithelial cells after repeated exposure to native mainstream smoke at the air-liquid interface, Exp. Toxicol. Pathol 69 (2017) 307–315. [PubMed: 28254108]

[31]. Merrifield J, O'Donnell R, Davies DE, Djukanovic R, Wilson SJ, A panel of antibodies for identifying squamous metaplasia in endobronchial biopsies from smokers, Biotech. Histochem 86 (2011) 340–344. [PubMed: 20662603]

[32]. Miller SJ, Lou DY, Seldin DC, Lane WS, Neel BG, Direct identification of PTEN phosphorylation sites, FEBS Lett. 528 (2002) 145–153. [PubMed: 12297295]

[33]. Earl J, Rico D, Carrillo-de-Santa-Pau E, Rodriguez-Santiago B, Mendez-Pertuz M, Auer H, Gomez G, Grossman HB, Pisano DG, Schulz WA, Perez-Jurado LA, Carrato A, Theodorescu D, Chanock S, Valencia A, Real FX, The UBC-40 Urothelial Bladder Cancer cell line index: a genomic resource for functional studies, BMC Genomics. 16 (2015) 403. [PubMed: 25997541]

[34]. Nickerson ML, Witte N, Im KM, Turan S, Owens C, Misner K, Tsang SX, Cai Z, Wu S, Dean M, Costello JC, Theodorescu D, Molecular analysis of urothelial cancer cell lines for modeling tumor biology and drug response, Oncogene. 36 (2017) 35–46. [PubMed: 27270441]

[35]. Cordier F, Chaffotte A, Terrien E, Préhaud C, Theillet FX, Delepierre M, Lafon M, Buc H, Wolff N, Ordered phosphorylation events in two independent cascades of the PTEN C-tail revealed by NMR, J. Am. Chem. Soc 134 (2012) 20533–20543. [PubMed: 23171049]

[36]. Fischer M, Census and evaluation of p53 target genes, Oncogene. 36 (2017) 3943–3956. [PubMed: 28288132]

[37]. Zhang ZT, Pak J, Huang HY, Shapiro E, Sun TT, Pellicer A, Wu XR, Role of Ha-ras activation in superficial papillary pathway of urothelial tumor formation, Oncogene. 20 (2001) 1973–1980. [PubMed: 11360181]

[38]. Tsuruta H, Kishimoto H, Sasaki T, Horie Y, Natsui M, Shibata Y, Hamada K, Yajima N, Kawahara K, Sasaki M, Tsuchiya N, Enomoto K, Mak TW, Nakano T, Habuchi T, Suzuki A, Hyperplasia and carcinomas in Pten-deficient mice and reduced PTEN protein in human bladder cancer patients, Cancer Res. 66 (2006) 8389–8396. [PubMed: 16951148]

[39]. Yoo LI, Liu DW, Le Vu S, Bronson RT, Wu H, Yuan J, Pten deficiency activates distinct downstream signaling pathways in a tissue-specific manner, Cancer Res. 66 (2006) 1929–1939. [PubMed: 16488991]

[40]. Zhou H, He F, Mendelsohn CL, Tang MS, Huang C, Wu XR, FGFR3b Extracellular Loop Mutation Lacks Tumorigenicity In Vivo but Collaborates with p53/pRB Deficiency to Induce High-grade Papillary Urothelial Carcinoma, Sci. Rep 6 (2016) 25596. [PubMed: 27157475]

[41]. Ahmad I, Singh LB, Foth M, Morris CA, Taketo MM, Wu XR, Leung HY, Sansom OJ, Iwata T, K-Ras and beta-catenin mutations cooperate with Fgfr3 mutations in mice to promote

Author Manuscript Author Manuscript Author Manuscript Author Manuscript

tumorigenesis in the skin and lung, but not in the bladder, Dis. Model Mech 4 (2011) 548–555. [PubMed: 21504907]

[42]. Zhou H, Huang HY, Shapiro E, Lepor H, Huang WC, Mohammadi M, Mohr I, Tang MS, Huang C, Wu XR, Urothelial tumor initiation requires deregulation of multiple signaling pathways: implications in target-based therapies, Carcinogenesis. 33 (2012) 770–780. [PubMed: 22287562]

[43]. Cheng J, Huang H, Pak J, Shapiro E, Sun TT, Cordon-Cardo C, Waldman FM, Wu XR, Allelic loss of p53 gene is associated with genesis and maintenance, but not invasion, of mouse carcinoma in situ of the bladder, Cancer Res. 63 (2003) 179–185. [PubMed: 12517796]

[44]. Castillo-Martin M, Domingo-Domenech J, Karni-Schmidt O, Matos T, Cordon-Cardo C, Molecular pathways of urothelial development and bladder tumorigenesis, Urol. Oncol 28 (2010) 401–408. [PubMed: 20610278]

[45]. Platt FM, Hurst CD, Taylor CF, Gregory WM, Harnden P, Knowles MA, Spectrum of phosphatidylinositol 3-kinase pathway gene alterations in bladder cancer, Clin. Cancer Res 15 (2009) 6008–6017. [PubMed: 19789314]

[46]. Koksal IT, Yasar D, Dirice E, Usta MF, Karauzum S, Luleci G, Baykara M, Sanlioglu S, Differential PTEN protein expression profiles in superficial versus invasive bladder cancers, Urol. Int 75 (2005) 102–106. [PubMed: 16123561]

[47]. Chen Z, Dempsey DR, Thomas SN, Hayward D, Bolduc DM, Cole PA, Molecular Features of Phosphatase and Tensin Homolog (PTEN) Regulation by C-terminal Phosphorylation, J. Biol. Chem 291 (2016) 14160–14169. [PubMed: 27226612]

[48]. Cordier F, Chaffotte A, Wolff N, Quantitative and dynamic analysis of PTEN phosphorylation by NMR, Methods. 77-78 (2015) 82–91. [PubMed: 25449899]

[49]. Fragoso R, Barata JT, Kinases, tails and more: regulation of PTEN function by phosphorylation, Methods. 77-78 (2015) 75–81. [PubMed: 25448482]

[50]. Chia YC, Catimel B, Lio DS, Ang CS, Peng B, Wu H, Zhu HJ, Cheng HC, The C-terminal tail inhibitory phosphorylation sites of PTEN regulate its intrinsic catalytic activity and the kinetics of its binding to phosphatidylinositol-4,5-bisphosphate, Arch. Biochem. Biophys 587 (2015) 48–60. [PubMed: 26471078]

[51]. Bolduc D, Rahdar M, Tu-Sekine B, Sivakumaren SC, Raben D, Amzel LM, Devreotes P, Gabelli SB, Cole P, Phosphorylation-mediated PTEN conformational closure and deactivation revealed with protein semisynthesis, Elife. 2 (2013) e00691. [PubMed: 23853711]

[52]. Shenoy SS, Nanda H, Losche M, Membrane association of the PTEN tumor suppressor: electrostatic interaction with phosphatidylserine-containing bilayers and regulatory role of the C-terminal tail, J. Struct. Biol 180 (2012) 394–408. [PubMed: 23073177]

[53]. Vazquez F, Ramaswamy S, Nakamura N, Sellers WR, Phosphorylation of the PTEN tail regulates protein stability and function, Mol. Cell. Biol 20 (2000) 5010–5018. [PubMed: 10866658]

Author Manuscript Author Manuscript Author Manuscript Author Manuscript

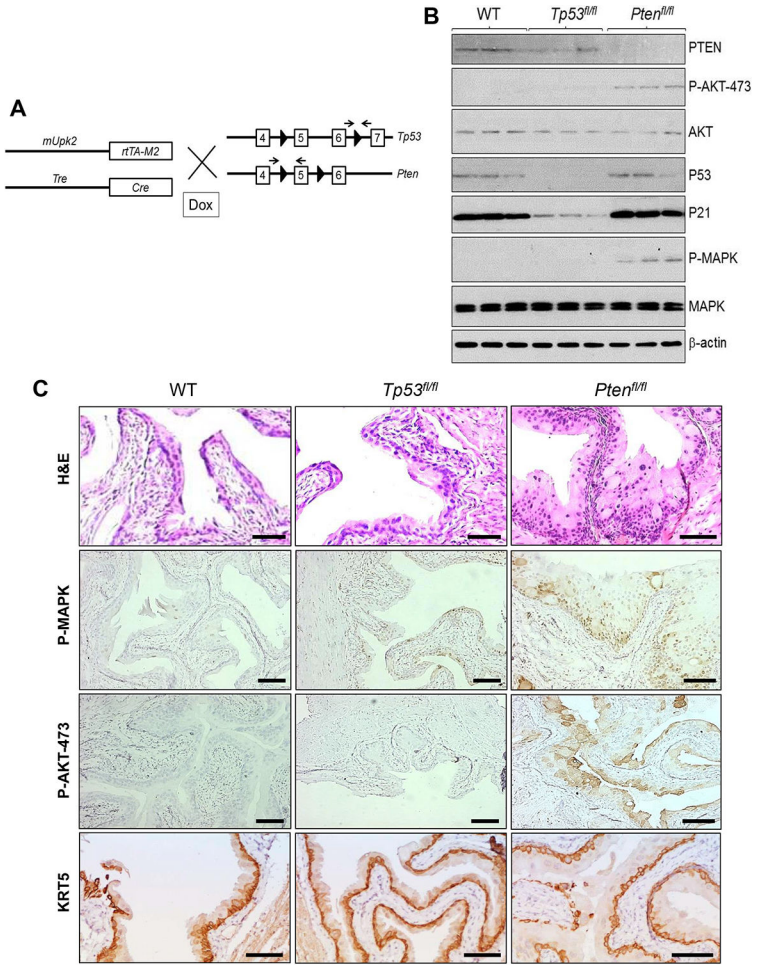

Figure 1.

(A) Strategy for time-controlled inactivation of *Tp53* or *Pten* in mouse urothelium. Double transgenic mice bearing (i) a 3.6-kb murine *Upk2* promoter which controls the expression of reverse tetracycline transactivator version M2 (*mUpk2-rtTA-M2*), and (ii) another transgene in which tetracycline-response elements control the expression of Cre recombinase (*Tre-Cre*) were crossed with a floxed p53 mouse line in which exons 5 and 6 of *Tp53* gene were flanked two loxP sites (arrowheads) or with a floxed *Pten* mouse line in which exon 5 of *Pten* gene was flanked with two loxP sites. Arrows denote oligonucleotide primer locations for genotyping purposes. Offspring after several additional crosses were subjected to doxycycline (DOX) treatment to activate *rtTA-M2* followed by *Cre* expression and subsequent ablation of *Tp53* or *Pten* in a time-dependent and urothelium-specific manner. Not all exons and introns of *Tp53* and *Pten* were included, and they were not drawn to proportion. (B) Western blotting of total urothelial protein extracts from wild-type (WT), floxed *Tp53* (*Tp53*$^{fl/fl}$) and floxed *Pten* (*Pten*$^{fl/fl}$) mice that also bore *mUpk2-rtTA-M2* and *Tre-Cre* transgenes (the latter two were omitted for brevity), using antibodies against the proteins shown on the right). Note the disappearance of PTEN and increased levels of phosphorylated AKT-473 and MAPK in *Pten*$^{fl/fl}$ mice and the disappearance of p53 and markedly decreased level of p21 in *Tp53*$^{fl/fl}$ mice. Total AKT, MAPK and β-actin served as loading controls. (C) Images representing the morphology(H&E) and expression

Author Manuscript Author Manuscript Author Manuscript Author Manuscript

of P-MAPK, P-AKT-473, and basal cell marker KRT5 in the urothelium of an 8-month-old wild-type (WT) mouse, an age-matched *Tp53*$^{fl/fl}$ mouse and an age-matched *Pten*$^{fl/fl}$ mouse. Note that the urothelia from the WT mouse and the *Tp53*$^{fl/fl}$ mouse were normal-looking, and the urothelium from *Pten*$^{fl/fl}$ mice was slightly hyperplastic and expressed increased amounts of P-MAPK and P-AKT-473. Scale bars in (C) equal to 100 μM.

Author Manuscript Author Manuscript Author Manuscript Author Manuscript

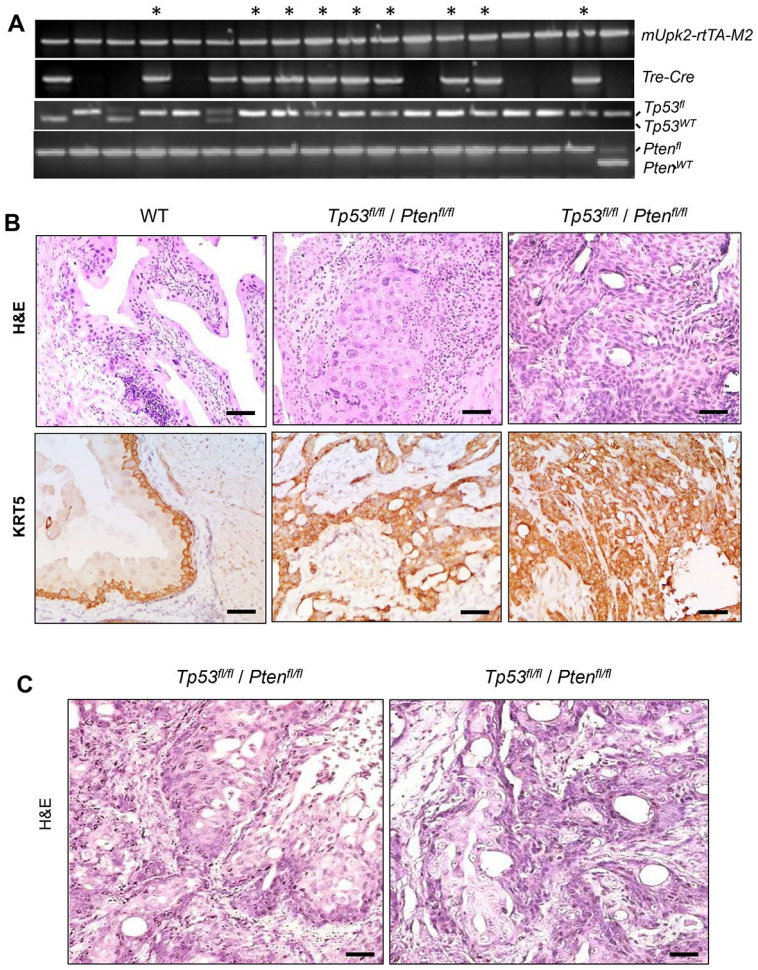

Figure 2.

Generation and analysis of double knockout mice lacking both *Tp53* and *Pten*. (A) Genotyping results of a mouse cohort with gene alleles marked on the right. Those bearing all the gene alleles, including both alleles of floxed $Tp53^{fl}$ and floxed $Pten^{fl}$, were indicated with * on the top. (B) Representative images of histology (H&E) and immunohistochemistry of anti-KRT5 showing normal urothelium from an 8-month-old, wild-type (WT) mouse and lesions of MIBC from two independent, aged matched $Tp53^{fl/fl}$ / $Pten^{fl/fl}$ double knockout mice. The invasive cells were strongly positive for KRT5 (C) Invasive lesions in the $Tp53^{fl/fl}$ / $Pten^{fl/fl}$ double knockout mice exhibited apparent squamous features. Scale bars in (B) and (C) equal to 50 μm.

Author Manuscript Author Manuscript Author Manuscript Author Manuscript

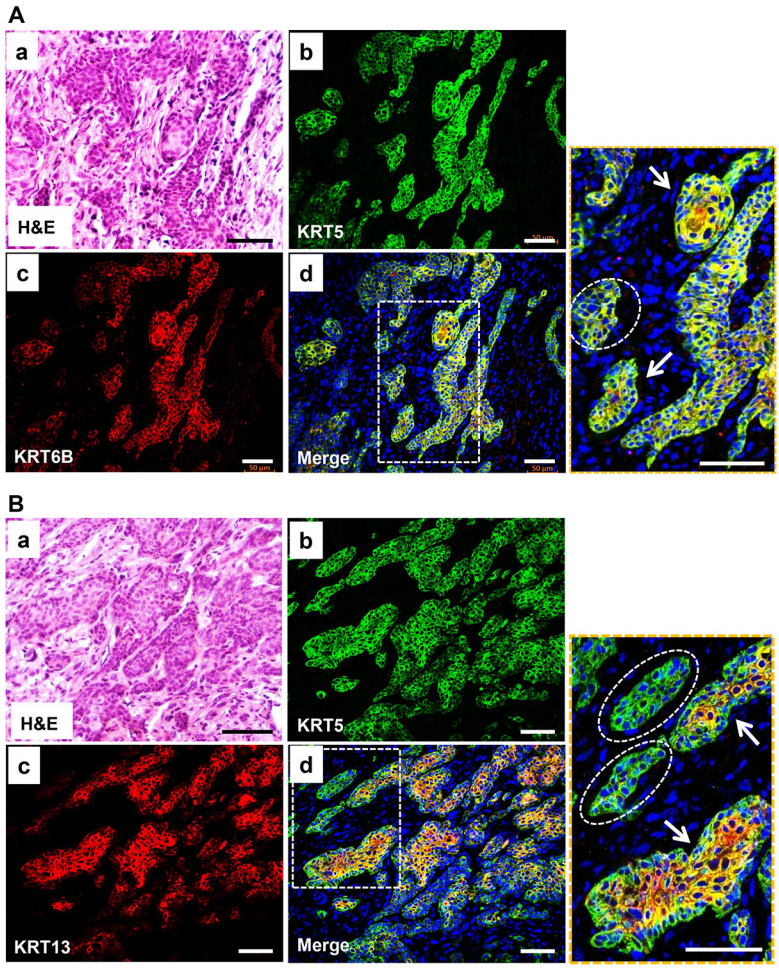

Figure 3.

Verification of squamous differentiation by double immunofluorescence phenotyping of MIBC in knockout mice lacking both *Tp53* and *Pten* using antibodies against squamous differentiation markers. Panels (A) and (B) served to show the labeling with squamous differentiation markers KRT6B and KRT13, respectively. Panels (a) within (A) and (B) were H&E staining performed after double immunofluorescence staining was completed and the photographs were taken for the exact match. Note that the invasive lesions were strongly positive for squamous differentiation markers, KRT6B (A) and KRT13 (B), and the staining matched well with that of basal marker KRT5, except that KRT5 was generally stronger in the basal cells, and KRT6B and KRT13 were stronger in the luminal cells (arrows) and were weak or absent in some of the tumor nests (dashed-line ovals). The scale bars equal to 50 μm.

Author Manuscript Author Manuscript Author Manuscript Author Manuscript

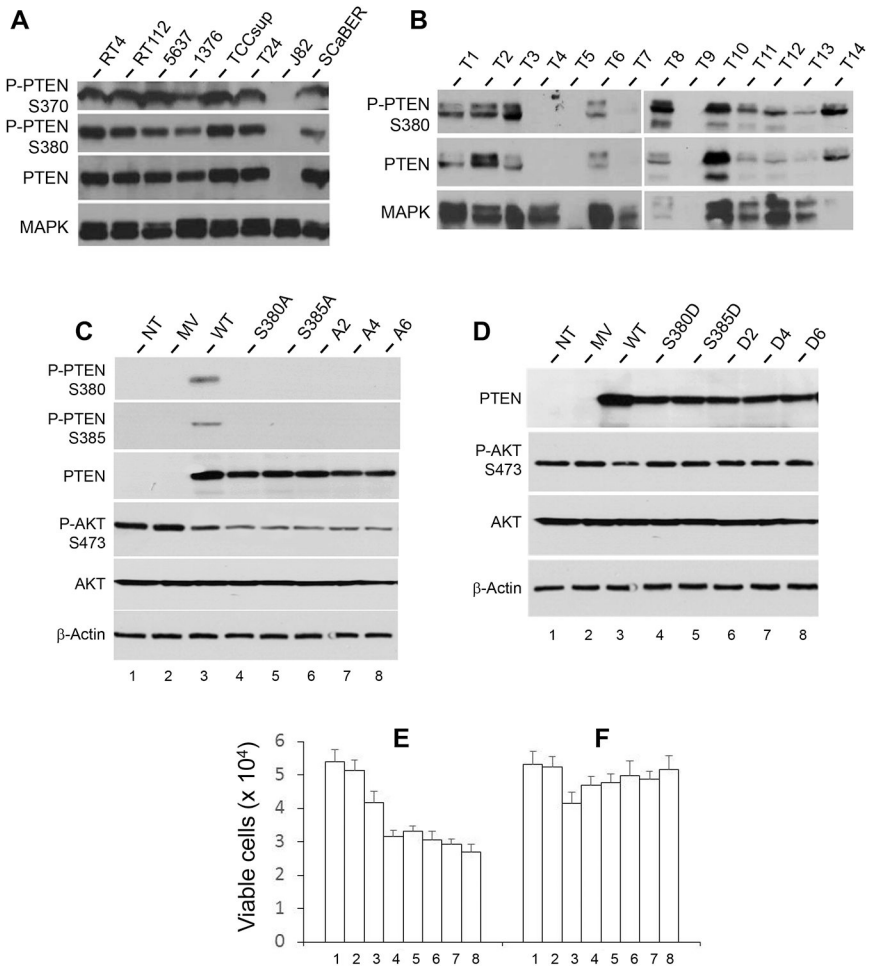

Figure 4.

PTEN status in human BC cell lines and specimens and effects of abolishing the C-terminal phosphorylation sites of PTEN. (A) Western-blot detection of PTEN and phosphorylated PTEN (S370 and S380) in a panel of established cell lines representing different grades and stages of human BC. Detection of MAPK served as a loading control. The lower three rows were from one western blot from which the prior antibody was completely stripped off, before another western blot was performed using a different antibody. The top row was from an independent western blot. Note that, with the exception of J82 cell line which had homozygous deletion of PTEN, all the other cell lines expressed PTEN, and all expressed PTEN was phosphorylated at S370 and S380. (B) Western-blot detection of PTEN and phosphorylated PTEN (S380) in a cohort of 14 snap-frozen, non-invasive human BC (T1-T7, low-grade and T8-T14, high-grade). The same western blot was used for blotting and re-blotting with different antibodies after complete stripping. Note the detection of PTEN and its C-terminal phosphorylation (S380) in all but two cases (T4 and T7). T5 and T9 were not informative due to protein degradation. (C and D) Site-directed mutagenesis was performed to replace the 6 potential phosphorylation sites (e.g., serines and threonines within the C-terminus (T366, S370, S380, T382, T383 and S385), singly or in several combinations, with alanine residues (C). The resultant cDNA expression vectors were transiently transfected into UMUC3 cells that lacked endogenous PTEN. The

Author Manuscript Author Manuscript Author Manuscript Author Manuscript

lane abbreviations were: NT, no transfection; MV, mock vector; WT, wild-type full-length PTEN; S380A, point mutation changing S380 to 380A; S385A, point mutation changing S385 to 385A; A2 (alanines replacing both S380 and S385); A4 (alanines replacing S370, S380, T382, T383 and S385); and A6, alanines replacing all the T366, S370, S380, T382, T383 and S385. The effects were assessed by western blotting of PTEN phosphorylation, AKT activation (C) and cell viability ((E), left 8 columns). Note that abolishment of one phosphorylation site (e.g., S380A) affected the phosphorylation of another site (S385) and vice versa. Also note that the lack of PTEN C-terminal phosphorylation led to increased inhibition on AKT phosphorylation (C; compare lanes 4-8 with lane 3) and a corresponding decrease in cell viability (E). Loss of additional phosphorylation sites on the C-terminus of PTEN (A4 and A6) showed similar results. (D) Site-directed mutagenesis and transient transfection were performed in parallel to those done in (C), except that the 6 potential phosphorylation sites of serine and threonine residues within the C-terminus were replaced, singly or in several combinations, with phosphorylation-mimicking aspartate(s). The abbreviations were NT, no transfection; MV, mock vector; WT, wild-type full-length PTEN; S380D, point mutation replacing S380 with 380D; S385D, point mutation replacing S385 with 385D; D2 (aspartates replacing both S380 and S385); D4 (aspartates replacing S370, S380, T382, T383 and S385); and D6, aspartates replacing all 6 C-terminal serine/threonine phosphorylation sites. Note that the expression of C-terminal phosphorylation mimetics of PTEN reduced the ability of PTEN to inhibit AKT activation (D, compare lanes 4-8 with lane 3) and increased cell viability as illustrated by the number of Trypan blue-unstained cells ((F), compared to (E)).

Author Manuscript Author Manuscript Author Manuscript Author Manuscript

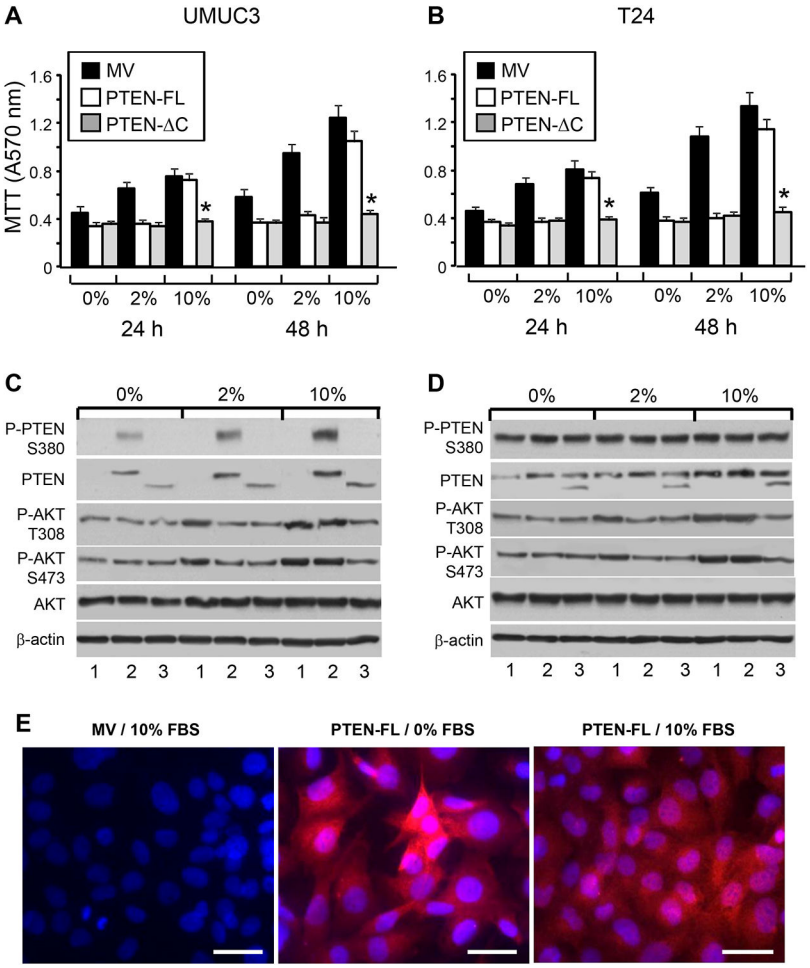

Figure 5.

Divergent cellular effects of full-length and tailless PTEN under different growth conditions. BC cell line UMUC3 that lacked endogenous PTEN (A and C) or T24 that expressed a mutated PTEN (B and D) were stably transfected with a mock vector (MV), that containing full-length PTEN (PTEN-FL), or that containing a tailless PTEN (PTEN-ΔC). The stably transfected cells were then grown in culture media containing 0, 2 or 10% FBS for 24h and 48h, and assessed for cell survival (A and B) or western blotting of PTEN and AKT phosphorylation status (C and D). Note that, in serum-free and FBS (2%) media, PTEN and tailless PTEN were equally effective in inhibiting cell survival. In high-serum (10%) media, however, tailless PTEN was a much more potent inhibitor than full-length PTEN, in both UMUC3 and T24 cells (A and B). The reduced inhibitory effects of full-length PTEN in high-FBS media corresponded well with increased C-terminal phosphorylation and decreased inhibition of AKT phosphorylation (C and D). (E) Immunofluorescent staining of stably transfected UMUC3 cells with mock vector or full-length PTEN showing the surface staining of PTEN in serum-free medium and cytoplasmic staining of PTEN in high-FBS medium. The scale bars equal to 50 μm.

Author Manuscript Author Manuscript Author Manuscript Author Manuscript

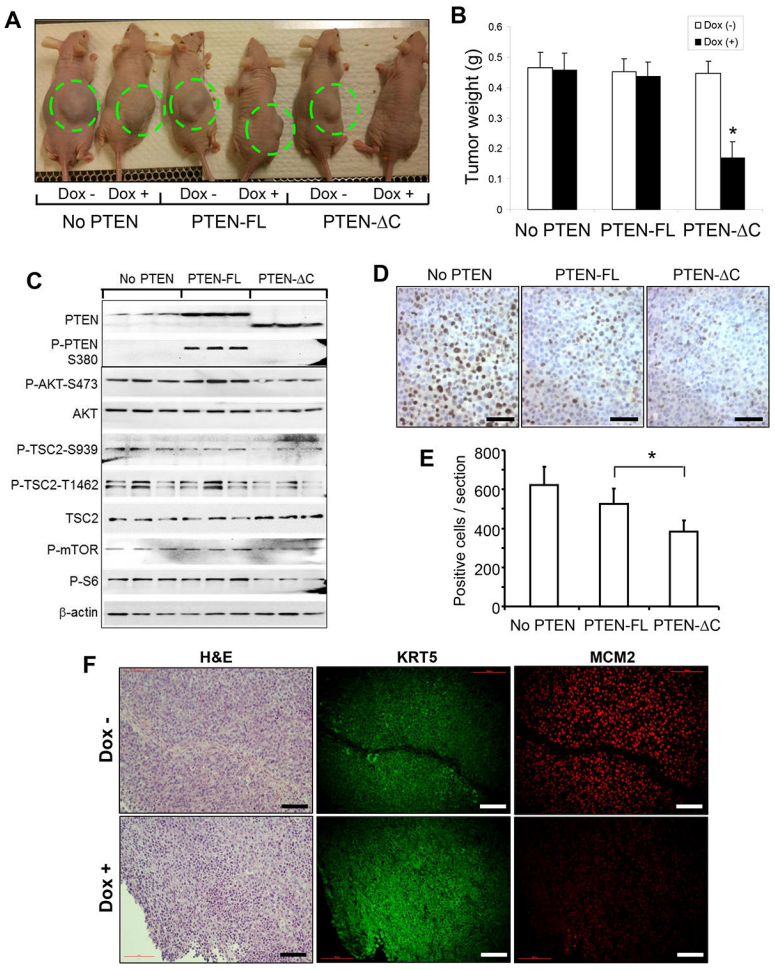

Figure 6.

Inhibition of tumor growth *in vivo* by inducible expression of tailless PTEN. Athymic nude mice were randomized into three groups (n=30/group), receiving subcutaneous injection of UMUC3 cells containing CMV-rtTA only, those containing both CMV-rtTA and TRE-PTEN-FL, or those containing both CMV-rtTA and TRE-PTEN-TL. Seven days after injection when visible tumors were seen, half of the mice (n=15) in each of aforementioned three groups continued to receive the regular diet, and another half of the mice (n=15) were switched to doxycycline-containing diet for two weeks after which all mice were enthanized. Note the marked reduction of tumor growth in the doxycycline-treated tailless PTEN group, compared to all the control groups (A and B). Also note the reduced phosphorylation of AKT, TSC2, mTOR and S6 in doxycycline-treated tailless PTEN group (C). The small amount of PTEN from the (No PTEN) controls may be originated from the non-tumor matrix cells from the mouse hosts that had grown into the tumor mass. Corresponding reduction of Ki-67 positive cells were also noted in the tailless PTEN-expressing group (D and E). Asterisks indicate statistically significant differences between the tailless and full-length PTEN groups. The scale bars in (D) equal to 100 μm. (F) Histology (H&E) and immunofluorescence staining of xenograft tumors bearing both CMV-rtTA and TRE-PTEN-TL that received the regular diet (Dox −) or doxycycline-containing diet (Dox +) as shown in (A). Note that the expression of MCM2 was much lower in the Dox + group that

Author Manuscript Author Manuscript Author Manuscript Author Manuscript

expressed the tailless PTEN than the Dox – group that did not express tailless PTEN. The scale bars in (D) equal to 100 μm.

Author Manuscript Author Manuscript Author Manuscript Author Manuscript

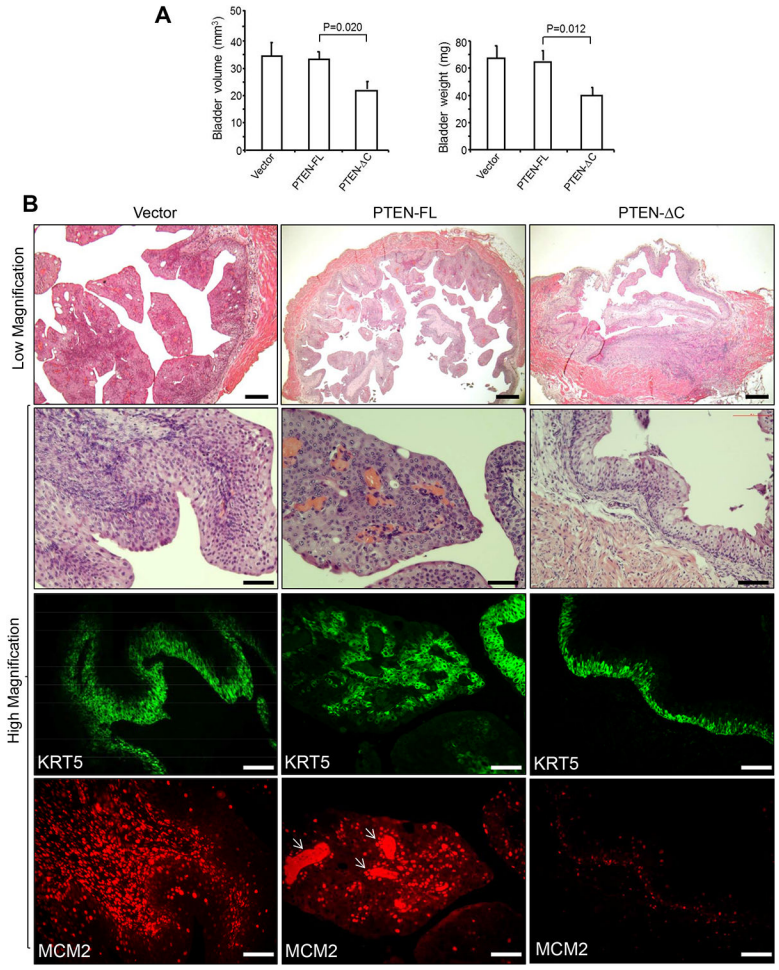

Figure 7.

Therapeutic effects of intravesical delivery of PTEN versus tailless PTEN. Transgenic mice (female, 5 months of age, n=5/vector) bearing two copies of *Upk2-HRas* mutant and developing non-muscle-invasive BC beyond 3 months of age [29] were instilled via the transurethral route adenovirus-driven vector (Vector), full length PTEN (PTEN-FL), or tailless PTEN. The mice were euthanized after three weeks of treatment (once per week), and their bladder sizes and weights (A), and histology was examined by H&E staining (top two rows) and protein expression (bottom two rows) by immunofluorescence staining (B). Note the significantly reduced bladder volume and weights in the tailless PTEN group, compared to the full-length PTEN group (A). Also note the hyperplastic changes in the tailless PTEN group, which expressed lower levels of MCM2 than in the tumor lesions of the Vector and full-length PTEN groups (B). Arrows in the bottom middle panel denote strong staining in the fibrovascular scores of tumor matrix whose components apparently were also undergoing active proliferation. The scale bars equal to 100 μm.

Author Manuscript

Author Manuscript

Author Manuscript

Author Manuscript

Table 1

Phenotypic alterations in adult mouse urothelia deficient for PTEN and/or p53

Dox	Genotype	6M	8M	10M	12M
Yes	UPII-rtTA-M2;TRE-Cre;PTEN$^{fl/fl}$	SH (10/10)	SH (10/10)	SH (12/12)	SH (14/14)
	UPII-rtTA-M2;TRE-Cre;p53$^{fl/fl}$	NU (9/9)	NU (11/11)	NU (12/12)	NU (13/13)
	UPII-rtTA-M2;TRE-Cre;PTEN$^{fl/WT}$;p53$^{fl/fl}$	NU (9/9)	NU (9/9)	NU (13/13)	NU (14/14)
	UPII-rtTA-M2;TRE-Cre;PTEN$^{fl/fl}$;p53$^{fl/WT}$	SH (9/9)	SH (11/11)	SH (14/14)	SH (13/13)
	UPII-rtTA-M2;TRE-Cre;PTEN$^{fl/fl}$;p53$^{fl/fl}$	MIBC (5/5)	MIBC (11/11)	ND	ND
No	UPII-rtTA-M2;TRE-Cre;PTEN$^{fl/fl}$;p53$^{fl/fl}$	ND	ND	NU (9/9)	NU (12/12)

NU: normal urothelium; SH: simple hyperplasia; ND: not determined